Journal of
Materials Chemistry B

Materials for biology and medicine

Accepted Manuscript

This article can be cited before page numbers have been issued, to do this please use: A. Muthaiah, K. Sakthivel, S. M. Chen and T. Chen, *J. Mater. Chem. B*, 2020, DOI: 10.1039/D0TB01324B.




ROYAL SOCIETY OF CHEMISTRY

rsc.li/materials-b

View Article Online
DOI: 10.1039/D0TB01324B

# FeMn Layered Double Hydroxides: An Efficient Bifunctional Electrocatalyst towards Real-time Tracking of Cysteine in Whole Blood and Dopamine in Biological Samples

Muthaiah Annalakshmi[1], Sakthivel Kumaravel[1,2], Shen-Ming Chen[1]*, Tse-Wei Chen[3]

[1]Department of Chemical Engineering and Biotechnology, National Taipei University of Technology, Taipei 106, Taiwan, ROC.

[2]Institute of Biochemical and Biomedical Engineering, National Taipei University of Technology, Taipei 106, Taiwan.

[3]Department of Materials, Imperial College London, London, UK

Corresponding Author: *Shen Ming Chen

E-mail: smchen78@ms15.hinet.net

View Article Online
DOI: 10.1039/D0TB01324B



## Abstract

A peculiar clock-regulated design of FeMn-LDHs (FMH) with specific physiochemical attributes has been developed and employed towards highly sensitive detection of cysteine (CySH) and dopamine (DA). The FMH nanoparticles were synthesized through a facile hydrothermal approach clocked at various (6 h, 12 h and 18 h) operating periods. Under optimal conditions, FMH are obtained in three unique morphologies such as hexagonal plate like, cubic, and spherical structures with corresponding to the clocked periods of 6 h, 12 h, and 18 h respectively. Among these, FMH-12 h possess the minimal particle size (54.45 nm), large surface area (7.60 $m^2/g$) and highest pore diameter (d = 4.614 nm). In addition to these superior physiochemical attributes, FMH nanocubes exhibits excellent electrochemical behaviors with lowest charge transfer resistance ($R_{ct}$; 96 Ω), high heterogeneous rate constant ($7.81\times10^{-6}$ cm $s^{-1}$) and good electroactive surface area (0.3613 $cm^2$), among the three. An electrochemical biosensor based on FMH nanocubes exhibits a remarkable catalytic activity toward CySH and DA with a lowest detection limit (9.6 nM and 5.3 nM), and broad linear range (30 nM-6.67 mM and 20 nM-700 μM). The FMH based biosensor is also feasible towards the real-world detection of CySH in whole blood and DA in biological fluids with satisfactory results. The proposed sensor possessed high selectivity, good repeatability, and reproducibility toward CySH and DA sensing.

**Keywords:** Layered double hydroxides, Neurotransmitter, Cysteine, Hydrothermal, Parkinson's disease, and bio-fluids.

View Article Online
DOI: 10.1039/D0TB01324B



## 1. Introduction

The quantitative analysis of physiologically most important biomolecules are thiols containing compounds of cysteine (CySH) and dopamine (DA) due to their wide biological significances, that are related with the regulation of physio-pathological functions in humans. DA is an essential neurotransmitter in synaptic communication between neuron cells, and widely existing in brain tissues, and body fluids of the mammals.[1] DA plays a vital role in transmitting information, and regulation of mammalian central nervous, cardiovascular, and renal systems. Further, it regulates the many day-to-day physiological activities in human body.[2] The fluctuations in the DA level can cause several neurological disorders including Parkinson's disease, schizophrenia, Tourette's syndrome, and Huntington's disease.[3] In addition, the consumptions of DA as an intravenous medication, which acts on the sympathetic nervous system, can lead to increasing blood pressure, and heart rates, etc.[4]

In addition to the detection of DA, the study of bio-thiols (CySH, homocysteine (Hcy) and glutathione (GSH)) provide a crucial role in physiological events and various diseases diagnosis. As one of the most important naturally occurring amino acid CySH plays a vital role in several biological process of cell metabolism, protein synthesis and detoxification and has been widely used in food and medicine industries.[5] CySH also serves as a potential biomarker and neurotoxin in various biomedical applications. The low concentration of CySH is directly associated with hair depigmentation, fat and muscle losses, liver damage, leucocyte, skin lesions and slow growth.[6] And also, CySH plays an important role in diagnosis of Alzheimer's and Parkinson's disease, cancer and immune deficiency syndrome.[7] Hence, the development of simple and effective protocols for the accurate quantification of CySH and DA in vivo/vitro is highly desirable in clinical and medical diagnosis.[6, 8] In tradition, a range of analytical techniques has been developed for the quantitative determination in natural complex biological samples. For example, chemiluminescence,[9] fluorescence spectrometry,[10, 11] high performance liquid chromatography,[12, 13] electrochemical methods,[14, 15] and ultraviolet–visible spectrophotometry.[16] Out of these methods, electrochemical strategies offer some intrinsic advantages such as low cost, high sensitivity,

View Article Online
DOI: 10.1039/D0TB01324B



portability and also extensively used for the practical analysis of the biosensors. Since they embrace certain intriguing skills of ease operation, high selectivity, and rapid response in biological systems.[17] In general, the direct electrochemical determination of DA and CySH in physiological fluids is still challenging. Due to the parallel oxidation potential of other bio-electroactive species such as ascorbic acid (AA), and uric acid (UA) may coexist with DA at much higher concentration levels (millimolar (mM) concentrations) than that of DA (0.01–1μM) and also the electroactive amino acids of GSH and Hcy are coexist with the CySH oxidation, which eventually leads to electrode fouling, lack of sensitivity, and selectivity.[18] Moreover, the electrochemical reaction of DA and CySH at bare electrodes is irreversible, need higher over potential, and offers poor reproducibility, due to the formation of oxidation products at the electrode surface.

To overcome these bottlenecks, numerous biologically recognized and tailored nanocomposites such as noble and non-noble metals/metal oxides/hydroxides and carbon-based materials have been developed as a potentially active electrocatalyst to improve the selectivity and sensitivity for the effective sensing of CySH and DA.[2, 19, 20] Nearly all of these developed biosensors approaches certain limitations, for example, as a high cost of noble meals, and natural enzymes are prone to be denatured and unstable in practical conditions. Further, these materials exhibit low detection limit, low sensitivity, and complex synthetic procedures involving consumption or exclusion of toxic chemicals. Therefore, an urgent need to develop a sustainable synthetic protocol with minimal or no consumption/emission of toxic substrates yet to offer an efficient electrocatalytic performance. Generally, non-noble metals are inexpensive, yet features offer good electrically conductive surfaces, high versatility in size, and shapes; blend all these attributes together they can offer a high electrocatalytic activity. Undoubtedly, transition metal (Mn, Fe, Ni, Co, Cu etc.) based oxides/hydroxides have been excellent electrocatalytic properties due to the high stability, superior redox behaviour, and large surface area.[20, 21]

Recently, layered double hydroxides (LDHs) has attracted a much more research interests due to their unique 2D brucite-like lamellar structures and excellent intrinsic properties includes ecofriendly, cheap, biocompatibility, abundant catalytic active sites, and chemical stability.[22] Generally, LDHs are cationic brucite like layered materials, which

View Article Online
DOI: 10.1039/D0TB01324B



containing both positively charged host layers and interlayer charge compensating anions and the structure of LDHs can be expressed as $M^{2+}_{1-x}M^{3+}_{X}(OH)_2]^{+}_{X}[A^{n-}_{x/n}.mH_2O]^{X}$, where, $M^{2+}$ and $M^{3+}$ are divalent and trivalent metal ions and $A^{n-}$ is a charge balancing anion.[23] In this structure, the divalent metal cations are coordinated in the octahedral position by the solvent (hydroxyl) molecules are substituted by trivalent metal cations and $A^{n-}$ can be various inorganic (like $Cl^-$, $NO_3^-$, $SO_4^{2-}$, etc.) or organic anions. LDHs have been widely used as an electrocatalyst in various fields such as energy storage, biosensors, and catalysis due to its high surface to volume ratio, more active sites per area, and high electron transfer ability.[24, 25] Especially, transition metal based LDHs (TM-LDHs) have been employed as an effective electrode material in multiple energy related applications and as it can easily undergo reversible redox reactions with in a potential range. Then the application of LDHs in electrochemical sensor is still limited when compared with its applications in electrochemical energy conversion, and storage systems.[26] Relevant cases such as Ni-Al-LDH/Graphene nanocomposites are efficiently used as an electrocatalyst for sensing application of dopamine due to its rich electroactive sites,[17] Chen et al., proposed the NiCo-LDH bearing Ni nanoparticle for amperometric determination of glucose,[27] Zhou et al., developed NiMn LDH/GO for the non-enzymatic electrochemical detection of $H_2O_2$ and glucose,[26] Y. Wang et al., proposed Ce-doped Mg–Al LDH toward the electrochemical determination of CySH[28] and Zhang et al., proposed CoFe LDH has been developed for the colorimetric determination of glucose and $H_2O_2$.[29] All the approaches proves that the TM-LDHs have been considered as an auspicious electrocatalyst toward the electrochemical sensing strategies. Generally, pure LDHs with unique morphologies are synthesized by the conventional, cost-effective co-precipitation induced under hydrothermal conditions in a closed system.[30] However, transition metals, especially $Fe^{3+}$, disposed to form gel like hydroxides at low pH values, making it difficult to synthesize TM-LDHs by homogeneous precipitation. In order to overcome this situation, hexamethylenetetramine (HMT) or urea were used as a hydrolysis agent, which makes the solution alkaline and induces homogeneous crystallization of LDH materials. However, the TM-LDHs have been synthesized by using urea-hydrolyzed method, the resultant product is typically contaminated with carbonate ions, thus limited their applications in many cases. But in the case of using HMT instead of urea, which favors the formation of ammonia at high

View Article Online
DOI: 10.1039/D0TB01324B

temperature, hence making the aqueous solution more alkaline.[31] The main advantages of the hydrothermal synthesis is that the resultant nanomaterial exhibits well crystallized structure with uniform particle size.

With this context, we planned to synthesis a FeMn LDHs (FMH) via hydrothermal route by using HMT as a hydrolysis agent and it can be used as an efficient electrode modifier for the electrochemical determination of CySH in human blood and DA in various biological fluids, with the key intentions focused on minimized overpotential, high selectivity, and sensitivity. Only few works had been developed on the basis of FMH such as Y. Ruan et.al. developed FMH for Oxygen evaluating phototherapy[32] and G. Huang et.al developed a FMH for cancer theranostics.[33] To the best of our knowledge, the first time to developing of FMH for the electrochemical sensor application, especially for CySH and DA determination. Hence, we demonstrated FMH has excellent sensing performances toward these biomolecules with rapid response, low detection limit, excellent selectivity, and also it applied for the real-world analysis (Scheme. 1).

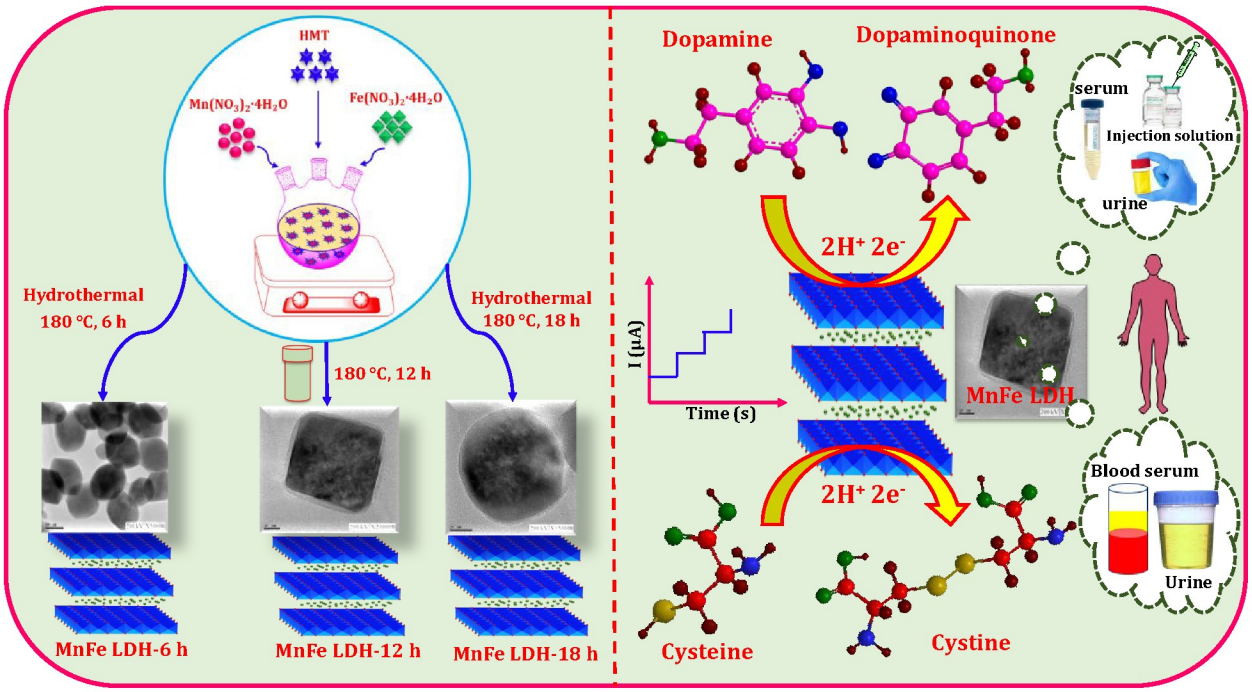


**Scheme 1.** Pictorial representation of the present work

View Article Online
DOI: 10.1039/D0TB01324B



## 2. Experimental section

### *2.1. Materials and methods*

Iron(III) nitrate nonahydrate ($Fe(NO_3)_3{\cdot}9H_2O$), manganese nitrate tetrahydrate ($Mn(NO_3)_2{\cdot}4H_2O$), hexamethylenetetramine (HMT), sodium dihydrogen phosphate ($NaH_2PO_4$), disodium hydrogen phosphate ($Na_2HPO_4$), sodium hydroxide (NaOH), dopamine hydrochloride, cysteine and ethanol ($C_2H_5OH$) were acquired from Sigma-Aldrich and used as received. The 0.05 M phosphate buffer solution (PBS) was prepared by mixing the two solutions of $Na_2HPO_4$ and $NaH_2PO_4$, was used as a supporting electrolyte for the all electrochemical experiments. Then the pH of this buffer solution was altered by adding $NaOH/H_2SO_4$. All the required solutions were prepared by using deionized water (DIW). For the real sample analysis, all the biological fluids (blood serum, urine and whole blood) were collected from Chang-Gung memorial hospital, Taiwan. Additionally, the test was approved by the institutional review board of Chang-Gung memorial hospital (IRB NO. 201801660B), Taiwan. Informed consents were obtained from human participants of this study.

The surface morphology of the as synthesized FeMn LDH (FMH) nanomaterials were surveyed by using transmission electron microscopy (TEM, JEOL 2001F) on TECNAI $G^2$ electron microscope using a 200kV accelerating voltage. The crystalline property of FMH was scrutinized through x-ray diffraction techniques (XRD, XPERT-PRO system with CuKα radiation; K = 1.54 Å). The X-ray photoelectron spectroscopy (XPS) were obtained on a Thermo scientific multilab 2000. The pore size distribution and specific surface area of the prepared samples were examined by using Brunauer-Emmett-Teller (BET) analysis. All the electrochemical performances were investigated by using CHI1205b electrochemical analyzer. The electrochemical impedance spectroscopy (EIS) was used to investigate the interfacial electrocatalytic property of the modified electrode was done in IM6ex (ZAHNER elektrik) within 0.01 to 100 kHz frequency at 0.2 V (AC potential: 5 mV). All the electrochemical measurements toward the determination of DA were performed by the all-in-one three-electrode system as glassy carbon electrode (GCE) with a geometrical surface area of 0.071$cm^2$ was used as a working electrode, saturated Ag/AgCl/Sat. KCl and platinum wire were used as a reference and auxiliary electrodes, respectively.

View Article Online
DOI: 10.1039/D0TB01324B



*2.2. Preparation and fabrication of FeMn LDHs*

The synthesis of FeMn LDHs (FMH) is carried out through the hydrothermal method. In a typical synthesis, a homogenous mixture of 0.02 M of $Mn(NO_3)_2{\cdot}4H_2O$ and 0.01 M $Fe(NO_3)_3{\cdot}9H_2O$ in 50 ml of DIW (2:1 ratio of $Mn^{2+}$ and $Fe^{3+}$) was treated with a solution of HMT (0.5 g/20 mL) in drops with constant stirring at room temperature. Thereafter, the reaction mixture was transferred into a 100 ml stainless-steel Teflon-lined autoclave and kept in a preheated oven at 180 °C; the autoclave was cooled down naturally to room temperature. The same synthetic procedure was repeated for various operating periods (6, 12 and 18h). The other ratios of $Mn^{2+}$ and $Fe^{3+}$ such as 1:1, 3:1 and 3:2 were synthesized at 180 °C for 12 h. After completion of reaction time, all the products were collected by centrifugation, thoroughly cleansed with DIW/ethanol, and dried in a hot air oven at 50 °C overnight to yield FMH. Prior to fabrication, the GCE was well polished with 0.05 mm alumina powder and washed thoroughly until get a mirror like surface by using DI water and ethanol. Then the synthesized FMH (4mg) was dispersed in 1 mL DI water and then ultra-sonicated for 30 min. After that, 6 µL of the FMH dispersion was drop-cast on the pre-cleaned surface of GCE and dried at 50 °C in a hot air oven. This fabricated electrode was used for the further electrochemical studies.

## 3. Results and discussion

*3.1. Structural and elemental characterizations of FeMn LDHs*

The surface morphological and crystallographic studies of as prepared nanomaterials (6 h – 18 h) were examined by transmission electron microscopy (TEM). The sizes of all the synthesized templates were obtained in nanoscale level and also, they are formed as uniform layered structures as depicted in Fig. 1A-C. Other $Mn^{2+}$: Fe molar ratios of precursors for the synthesis of FeMn-LDH (FMH), such as 1:1, 3:1, and 3:2, were also investigated. However, these precursor ratios created FMH with relatively irregular morphology (Fig. S1). Therefore, we only investigate the MnFe-LDH synthesized with a 2:1 precursor ratio in the subsequent experiments. The TEM image of Fig. 1A (FMH-6 h) shows a uniform distribution of hexagonal plate like structure with the average particle size up to 82.4 nm. On the other hand, FMH-12 h (Fig. 1B) has the homogenously distributed cubic particles with an average

View Article Online
DOI: 10.1039/D0TB01324B



particle size of 54.45 nm. At last, as we increasing the reaction time up to 18 h, the FMH shows the spherical structure with the average particle size is 79.02 nm (Fig. 1C). Compared with these different structures, the FMH-12 h has very low average particles size.

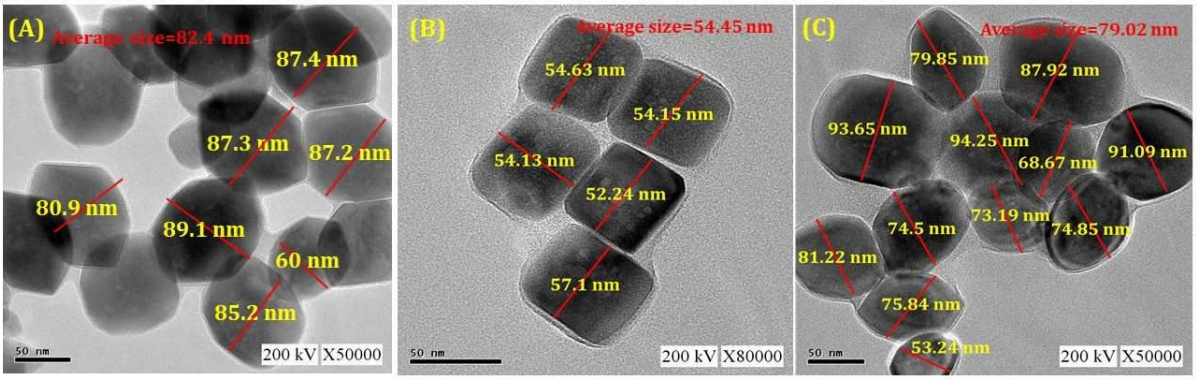


**Fig. 1.** TEM images of FMH-6 (A), FMH-12 h (B) and FMH-18 h (C).

Additionally, $N_2$ adsorption and desorption isotherm for FMH (6, 12, and 18 h) was analyzed to find the pore distribution and surface area, were shown in Fig. S2A-F. As can be seen from Fig. S2A-C, all the prepared FMH samples possess mesoporous structure and the shape of the $N_2$ sorption isotherm can be identified as a type IV with low sorption loop at the relative pressure ($P/P_0$) of 0.30. Then the corresponding surface area of FMH samples were to be 7.52 (6 h), 7.60 (12 h), and 7.37 (18 h) $m^2/g$ respectively. As we known, the lowest particle size and highest surface area has the highest electrocatalytic activity. Then, the pore distribution of proposed samples was identified by using Barrett–Joyner–Halenda (BJH) model, and the results were illustrated in Fig. S2D-F. From this profile, the average pore diameter (D) was calculated for FMH-6h (d =4.032 nm), 12 h (d = 4.614 nm), and 18 h (V =d = 4.2395 nm) respectively. From this result, the obtained FMH-12 h has more porous surface, and higher specific surface area when compared to others, thus facilitate the rapid electron transfer and relatively enhance the electrocatalytic behavior. Hence, we chosen the FMH-12 h nanocubes for the further electrochemical studies.

To further investigate the more morphological properties of FMH-12 h was studied from TEM analysis. The different magnification of TEM images of FMH-12 h were displayed in Fig. 2A-C, which revealed the homogeneous distribution of FMH nanocubes were formed with the uniform size and shape. Fig. 2D clearly shows that the presence of Fe, Mn and O in

View Article Online
DOI: 10.1039/D0TB01324B



FMH nanocubes. The selective area diffraction (SAED) pattern (Fig. 2E) shows the formation of FMH with corresponding planes are (006) and (009), respectively, which mimics with the XRD pattern. Further, the reported HRTEM (Fig. 2F) images further confirming the prepared FMH and the "d" spacing value of lattice fringes was calculated to be 0.74, which is correspond to the planes of (003). Further, the energy dispersive elemental mapping (EDS) were confirms the presence and homogeneous distribution of Fe, Mn, O in the FMH nanocubes, was shown in Fig. S3A-E.

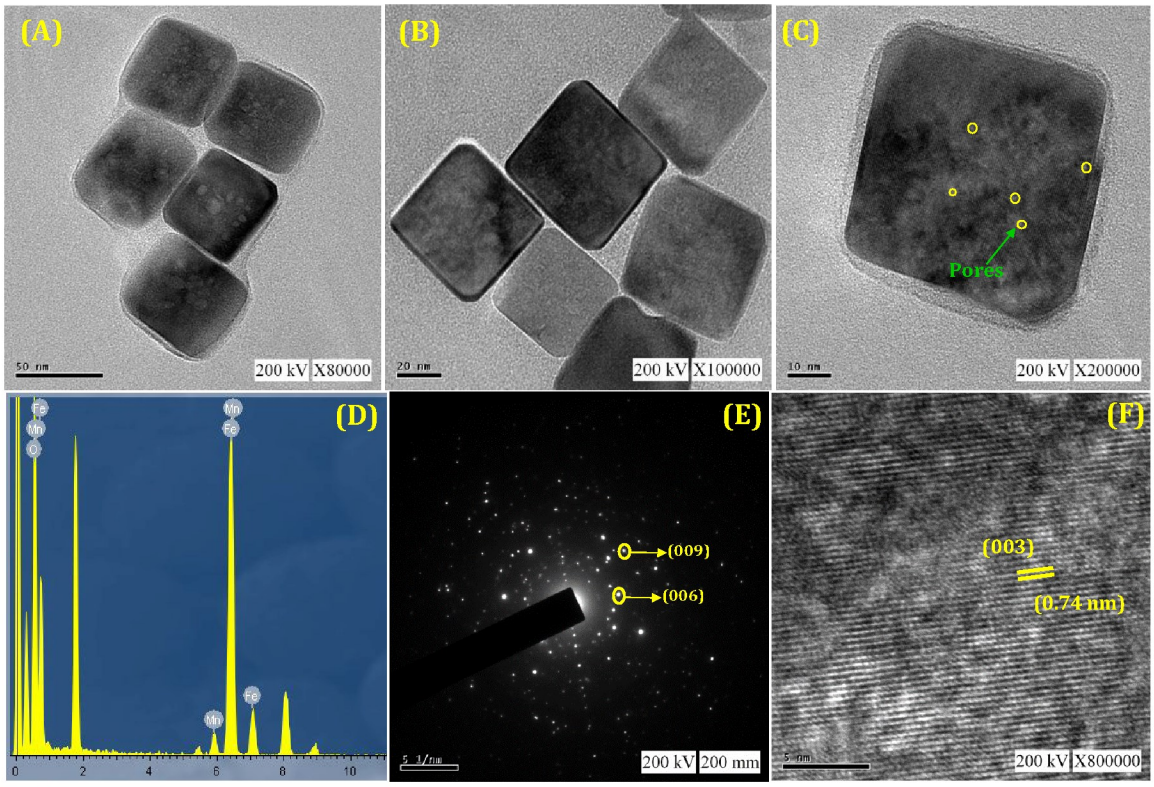


**Fig. 2.** Different magnified TEM images (A-C), EDX (D), SAED pattern (E), HRTEM image (F) of FMH-12 h nanocubes.

The crystalline structure and the formation of FMH has been further confirmed through X-ray diffraction techniques, was revealed in Fig. 3A. It portrays the characteristic diffraction peaks at 11.93, 22.36 and 34.6 and are relevant to the lattice planes of (003), (006) and (009) respectively, which are the characteristics of layered structures, confirming the hydrotalcite-like LDH structure and it was perfectly matched with the standard diffraction data (JCPDS card no. 38-0715), also well accordance with the previous literatures.[32, 33] The ($d_{003}$) spacing

View Article Online
DOI: 10.1039/D0TB01324B



of MnFe-LDH was found to be 0.74 nm, which is indexed with the interbrucite like LDH phase on the basis of Braggs law.[34] Furthermore, there are no other crystalline phase were observed, which emphasize a high purity of FMH. In order to characterize the exact valence state of the elements, XPS analysis was achieved and reported the obtained high-resolution XPS spectra in Fig. 3B-D. In this, Fig. 3B exhibits the XPS survey spectrum of FMH, confirmed the presence of C, O, Mn, Fe. The high-resolution XPS spectra of Fe 2p (Fig. 3C) depicts the binding energy of 712.3 and 725.4 eV for Fe $2p_{3/2}$ and Fe $2p_{1/2}$, which validates the presence of $Fe^{3+}$.[32] Meanwhile, the high-resolution XPS spectra of Mn 2p (Fig. 3D) shows the Mn $2p_{3/2}$ and Mn $2p_{1/2}$ peaks at the binding energy of 643 and 654.9 eV respectively, indicating the presence of $Mn^{2+/4+}$.[35]

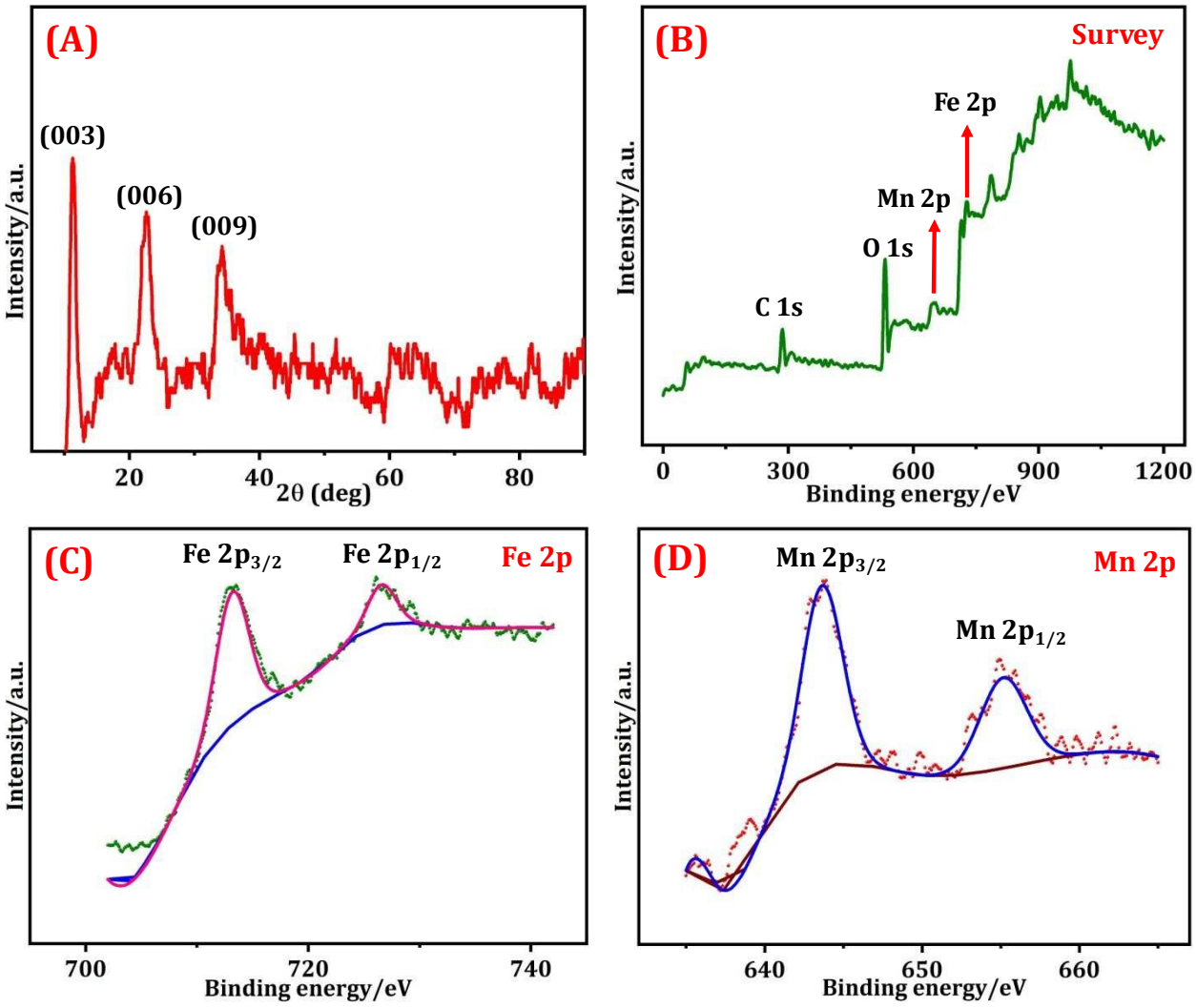

View Article Online
DOI: 10.1039/D0TB01324B

**Fig. 3.** XRD pattern for FMH (A), XPS survey (B), Fe 2p (C) and Mn 2p (D) spectrum of FMH nanocubes.

*3.2. Electrochemical characteristics of modified electrodes*

In order to characterize the electrochemical attributes and rate of electron transfer for the different FMH modified electrodes, electrochemical impedance spectroscopy (EIS) was performed. The impedance data was recorded for all the prepared samples of FMH in 0.1 M KCl containing 5 mM $[Fe(CN)_6]^{3-/4-}$ in the frequency range of 0.1 Hz to 100 kHz at an AC applied potential (10 mV) (Fig. 4A). In the Nyquist plot, the semicircle region appeared at higher frequencies can reflect the behavior of electron transfer process and the linear region at lower frequencies is related to the diffusion process on the electrode surface.[36] The diameter of this semicircle corresponds to the electron transfer resistance ($R_{ct}$) at the interface of electrolyte/electrode. The value of $R_{ct}$ will be varied with the different substances. As shown the top left inset of Fig. 4A represents the Randle's equivalent circuit, which used to fit the Nyquist plot. Where, $R_s$ is the electrolyte resistance, $R_{ct}$ is the charge (electron) transfer resistance and $Z_w$ is the Warburg impedance and $C_{dl}$ is the interface capacitance. From Fig. 4A, FMH-6 h (curve a) displays a large semicircle at higher frequencies, indicating the large electron transfer resistance. In contrast, the semicircle diameter was significantly changed for after modification of GCE with FMH- 12 h (curve b), and 18 h (curve c), respectively. From this result, the calculated $R_{ct}$ value of FMH/GCE (6 h), (12 h), and (18 h) is about 244 Ω, 96 Ω, and 152 Ω, respectively. As anticipated, the lowest $R_{ct}$ was obtained for FMH/GCE- 12 h nanocubes than others courtesy of its high surface area and porosity, which could effectively facilitate the electron transfer rate on the electrode surface. These results clearly proved that the enhanced electrochemical behavior of FMH (12 h) nanocubes has been significantly improved by the excellent surface area, good ionic conductivity.

Consequently, the heterogeneous rate constant ($k_s$) of all the modified electrodes can be calculated based on the obtained $R_{ct}$ by using the following Eq. (1).[37]

$$R_{ct} = RT/n^2F^2Ck_s \quad \text{---------- (1)}$$

View Article Online
DOI: 10.1039/D0TB01324B



From this Eq. (1), R, T, n, F and C represents the gas constant (8.314 J $mol^{-1}$ $K^{-1}$), room temperature (298 K), number of electrons involved, Faraday constant (96485 C/mol) and concentration of $[Fe(CN)_6]^{3-/4-}$ in bulk solution. By using the above Eq. (1), the obtained $k_s$ for FMH-6 h (a), FMH-12 h (b) and FMH-18 h (c) are to be $3.02\times10^{-6}$, $7.81\times10^{-6}$ and $4.9\times10^{-6}$ cm $s^{-1}$, respectively.

To further examine the electrocatalytic activity of the FMH nanocubes, CV was performed in 0.1 M KCl containing 5 mM $[Fe(CN)_6]^{3-/4-}$ at a scan rate of 50 mV $s^{-1}$. As can be seen from the depicted Fig. 4B, the bare GCE (a) reveals a quasi-reversible redox behavior with a peak to peak separation of 125 mV ($\Delta E_p$). Moreover, a distinct redox peaks and lowest peak to peak separations (differences between cathodic ($E_{pc}$) and anodic ($E_{pa}$) peak potential) was observed for all modified electrodes are to be FMH-6 h/GCE ($\Delta E_p$= 108 mV), FMH-12 h/GCE ($\Delta E_p$= 104 mV), and FMH-18 h/GCE ($\Delta E_p$= 107 mV), respectively, when compared to bare GCE. While, the significant increases were obtained in the redox peak current for all FMH/GCE. The ratio of cathodic and anodic peak current response ($I_{pc}/I_{pa}$) for bare GCE (curve a), FMH-6 h/GCE (curve b), FMH-12 h/GCE (curve c) and FMH-18 h/GCE (curve d) are 0.9821, 0.9869, 1.002 and 1.0063, respectively. The redox peak current ratio of FMH-12 h/GCE (1.002) is well ascribed with the theoretical redox peak current ratio of the reversible reaction is 1.[38] The lowest $\Delta E_p$ and the highest $I_{pc}/I_{pa}$ of FMH-12h/GCE may be due to their rapid electron transferring rate and high surface area. Further, the CV was obtained at various scanning rate (20-200 $mVs^{-1}$) at FMH-12 h/GCE, revealed in Fig. 4C, in which the redox peak current increases gradually while increasing the scan rates. As shown Fig. 4D shows the linear relationships of the redox peak currents ($I_{pc}/I_{pa}$) along with the square root of the scan rate ($\nu^{1/2}$) and the correlation coefficient ($R^2$) values are 0.9915 and 0.9938 respectively, demonstrating the electrochemical process of ferricyanide is diffusion-controlled process at the modified electrode.[39]

The electrochemical surface area can be calculated by the following Randles-Sevcik equation [eq.2].[40]

$$I_p = (2.69\text{x}10^5)AD_0^{1/2}\, n^{3/2}C_0\nu^{1/2} \text{---------- (2)}$$

View Article Online
DOI: 10.1039/D0TB01324B



Where, $I_p$ is the anodic or cathodic peak current, A is electroactive surface area, $D_0$ is the diffusion coefficient ($6.67\times 10^6$ $cm^2/s$) of $[Fe(CN)_6]^{3-/4-}$, n is the number of electron transfer in the reaction, $C_0$ is the concentration of ferricyanide (5 mM), and ν is the scan rate. The electrochemical active surface area can be calculated by using the slope of the obtained linear plot and the calculated values are 0.071, 0.127, 0.3613, and 0.167, $cm^2$ respectively. To conclude, FMH-12 h has the highest electroactive surface area. According to these above results, FMH-12 h was chosen as a better electrocatalyst towards the detection of CySH and DA. Hence, all the electrochemical studies were done at FMH-12 h modified electrode.

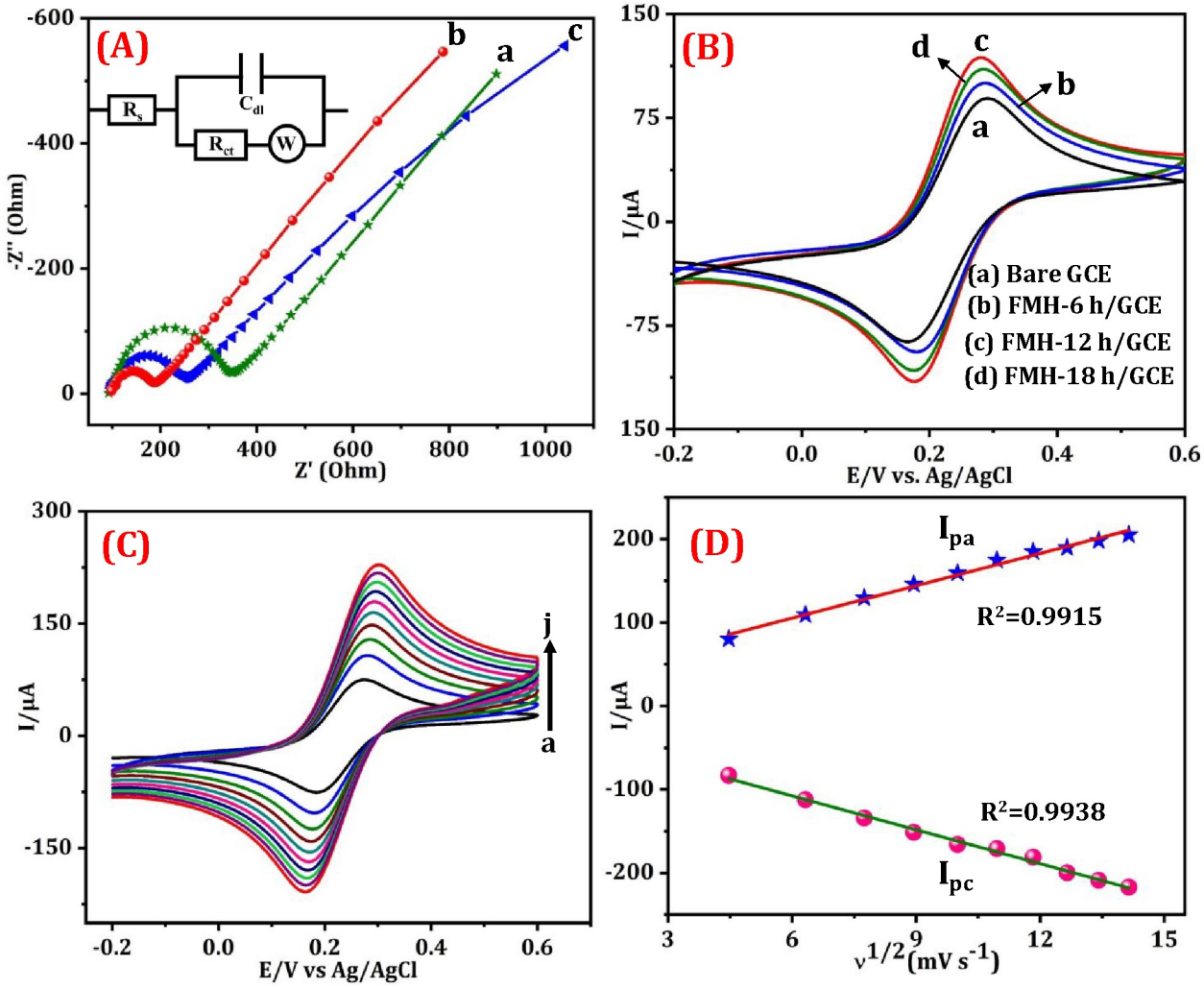


**Fig. 4.** (A) EIS of FMH-6h/GCE (a), FMH-12 h/GCE (b) and FMH-18 h/GCE (c) in 0.1 M KCl containing 5 mM $[Fe(CN)_6]^{3-/4-}$. (B) CV responses of bare GCE (a), FMH-6h/GCE (b), FMH-12 h/GCE (c) and FMH-18 h/GCE (d) in 5 mM of $[Fe\ (CN)_6]^{3-/4-}$ containing 0.1 M KCl at a scan

View Article Online
DOI: 10.1039/D0TB01324B



rate of 50 mV $s^{-1}$. (C) CV responses of FMH-12 h/GCE in 5 mM of $[Fe(CN)_6]^{3-/4-}$ containing 0.1 M KCl at different scan rate from 20 to 200 mV $s^{-1}$ (a→j). (D) The linear plot between the redox peak current *vs.* square root of scan rate.

### *3.3. Electrocatalytic detection of DA at FMH modified electrode*

#### *3.3.1. Electrocatalytic performances of FMH modified electrode towards DA*

Before the electrochemical experiments, loading amount of catalyst on electrode surface should optimized because it could be affect the sensitivity of the electrode. Hence, the various amount of FMH dispersion (2, 4, 6, 8, 10 µL) was loaded on GCE, dried at room temperature and obtain CV for 200 µM DA and 0.3 mM CySH in PBS (pH 7). The obtained current responses were shown in Fig. S4A&B. It can be seen that 6 µL FMH dispersion loaded electrode exhibited an increased response current toward DA and CySH than that of other conditions. Hence, 6 µL FMH dispersion loaded electrode was used for further electrochemical investigation.

The electrocatalytic activity of modified and unmodified GCE towards the electrochemical oxidation of DA was investigated by CV in 0.05 M PBS (pH 7) at a scanning rate of 50 mV $s^{-1}$. Fig. 5A reveals the outcome of CV responses of bare GCE and FMH/GCE toward 200 µM DA. Obviously, no redox peaks were observed on bare GCE (curve a) and FMH (curve b) in the absence of DA, Fig. 5A. In contrast, in presence of 200 µM DA at bare GCE (curve a'), a pair of weak and broad irreversible redox peaks was appeared at $E_{pa}$=0.28 V and $E_{pc}$=0.14 V, respectively. Moreover, the observed anodic ($I_{pa}$) and cathodic ($I_{pc}$) peak current values are to be 4.75 and 2.72 µA, respectively, indicating that the electrocatalytic process of DA is sluggish at bare GCE. However, the prominent redox pair was appeared on FMH/GCE toward 200 µM DA at 0.2 ($E_{pa}$) and 0.19 V ($E_{pc}$), respectively, and its $I_{pa}$ (27 µA) and $I_{pc}$ (17.6 µA) were respectively about 5.7 and 6.5-fold higher than bare GCE, indicates the superior electrocatalytic behavior of FMH nanocubes towards DA. Obviously, the decrease in the peak potential and dramatic increase in the current responses can be attributed to the structure with high porosity of FMH nanocubes, which providing more active sites, and high adsorption capacity (rapid oxidation) of DA at electrode surface.

#### *3.3.2. Effect of scan rate towards DA at FMH modified electrode*

View Article Online
DOI: 10.1039/D0TB01324B



In order to investigate the reaction kinetics and transport characteristics of the electrochemical oxidation of DA on FMH modified GCE, CV was performed in 0.05 M PBS (pH 7) containing 200 μM DA at different scan rates (20-200 mV $s^{-1}$). The Fig. 5B displays the redox peak currents of DA increased gradually while increasing the scan rate (20-200 mV $s^{-1}$) and a slow simultaneous study shift takes place in the redox peak potential towards positive side, demonstrating the rapid electron transfer kinetics across the surface of the electrode and the electrochemical oxidation of DA is a quasi-reversible process. The calibration plot of redox peak current ($I_{pa}$, $I_{pc}$) as a function of scan rate (ν) exhibits a linear relationship and the obtained linear regression coefficients are $R^2$ = 0.9972 ($I_{pa}$) and $R^2$ = 0.9994 ($I_{pc}$), respectively (Fig. 5C). These results justify that the electrochemical oxidation of DA is a typical adsorption-controlled process.

According to the Laviron's equations, we can calculate the number of electrons transferred in the reaction [eq.3].[41]

$$I_p = n^2F^2\nu A\Gamma_T/4RT = nFQ\nu/4RT,\ Q = nFA\Gamma_T \quad \text{---------- (3)}$$

Where, n denotes the number of electrons transferred, F represents the Faraday constant, Q is the peak area (calculated by the charges in C), A is the electrode area and ν is the corresponding scan rate. The n value can be calculated by using the slope value of I versus ν, the obtained n values are 1.68 and 1.82, respectively, therefore, the value of n is approximately 2. Then the charge transfer coefficient (α) was also calculated by using following equation [eq.4].[41]

$$E_p = E_0 + RT/(1-\alpha)nF\ \ln\nu \quad \text{---------- (4)}$$

The relationship between $E_{pa}$ and lnν for the DA oxidation is depicted Fig. S3A, where the linear equation with regression coefficient is $R^2$=0.9925. By using this slope value, the α value was calculated is to be 0.54. Based on this above result, the electrochemical oxidation of DA is a two electron, and two-proton transfer reaction. The reaction mechanism of the dopamine oxidation can be written as follows.

View Article Online
DOI: 10.1039/D0TB01324B

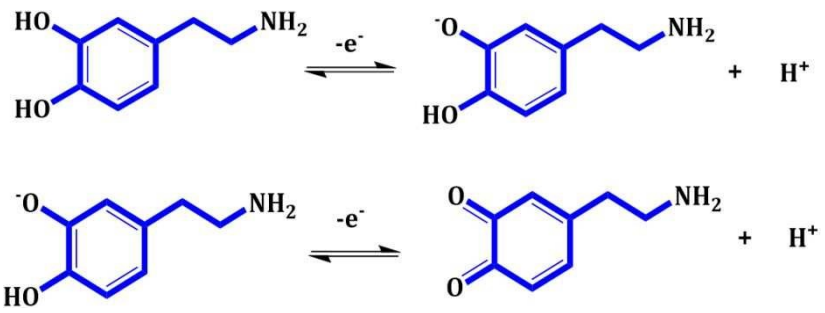


In this electrocatalytic oxidation of DA, the semi-quinone radical was formed as the intermediate in the first step by losing of one proton and one electron. Next, the quinone produced at the second step with further releasing of one proton and one electron from the intermediate product, can be seen from the above reactions.

*3.3.3. Amperometric determination of DA at FMH modified electrode*

In order to explore the quantitative dynamic range and response efficacy of FMH modified electrode, amperometric i-t experiments was carried out for various concentrations of DA in 0.05 M PBS (pH 7) with constant stirring (1600 rpm) by rotating disk electrode (RDE). The study of amperometric assays is more sensitive and it's mainly dependent on the applied potential, which has a significant effect on the selectivity and sensitivity of the electrochemical reactions. The maximum response current was attained at 0.2 V; hence, it was chosen as the optimal potential for DA detection. The Fig. 5D indicates the i-t responses of FMH modified electrode with the consecutive addition of DA. The steady state current response was attained within 2 s. Under optimal conditions, the current responses were linearly increased for the consecutive additions of DA (20 nM-700 μM) into the electrolyte solution, revealed in Fig. 5D. The sensor exhibits two linearity, the concentration ranges from 20 nM to 3.9 μM for lower level and 3.9 μM to 700 μM for higher concentration. The linear plot of anodic peak current ($I_{pa}$) versus various mass fraction of DA with the linear regression coefficient ($R^2$ = 0.9921 and 0.996), was displayed in Fig. 5E. The limit of detection (LOD) and limit of quantification (LOQ) was calculated to be 5.3 nM and 17.6 nM by using the formula LOD = 3 $S_a$/b and LOQ= 10 $S_a$/b, under a signal-to-noise ratio of 3 (S/N = 3),[42] where, $S_a$ is the standard deviation of the intercept and b is the slope of the linear plot. When the concentration of DA increases to 700 μM, it is found that the amperometric current response reaches saturation gradually, indicating that all active sites

View Article Online
DOI: 10.1039/D0TB01324B

of the electrode are covered with reaction intermediates at high concentration of DA. The electrochemical performances of the proposed sensor are superior to those of previously reported DA sensors, tabulated in Table S1. These results clearly show that the analytical parameters of linear range and LOD at FMH modified electrode are better than those proposed DA sensors at different modified electrodes. The excellent electrochemical activity is due to the following physiochemical attributes of unique structure of FMH nanocubes possess large surface area; it has more active sites, thus could enhance the ionic conductivity of FMH. Which allowing the rapid electron transfer amongst the electrolyte and electrode surface. Therefore, FMH modified GCE can be used as an excellent electrocatalyst toward DA determination in clinical diagnosis and cellular investigation.

*3.3.4. Anti-interference study toward DA oxidation*

Selectivity is the major challenge for all non-enzymatic sensing applications, because human fluids containing rich electroactive substrates with redox profiles at similar oxidation potentials. So as to study the influence of interfering species toward the DA detection, amperometric it experiments was performed on FMH modified electrode in presence of various possible interfering species including ascorbic acid (AA), uric acid (UA), citric acid (CA), glycine (gly), glucose (glu), cysteine (cys), lysine (lys), aspartic acid (Asp) $K^+$, $Na^+$, $Cl^-$ $NO_3^-$ and $SO_4^{2-}$. The experiments were carried out by taking 20-fold concentration of UA, AA and 100-fold higher concentration of CA, gly, glu, cys, lys and Asp, then $K^+$, $Na^+$, $Cl^-$ $NO_3^-$ and $SO_4^{2-}$ (<500-fold) in the presence of 100 μM DA in 0.05 M PBS (pH 7), was shown in Fig. 5F. Obviously, the current responses of DA increased progressively for each addition of 100 μM DA. As well known that the anodic peak potentials for UA, AA, and DA are very close to one another, thus may overlapping with each other during the electrochemical process. From Fig. 5F clearly proves that the presence of UA (a) and AA (b) did not interfered in the detection of DA at this potential. Additionally, other common coexisting compounds such as CA (c), gly (d), glu (e), cys (f), lys (g), Asp (h), $K^+$ (i), $Na^+$ (j), $Cl^-$ (k), $NO_3^-$ (l) and $SO_4^{2-}$ (m) were also not able to produce any sizable change in the anodic peak current response of DA, as revealed in Fig. 5F. These results clearly demonstrate that our proposed FMH modified GCE possess good selectivity for the quantitative determination of DA and good tolerance towards common biological interferences.

View Article Online
DOI: 10.1039/D0TB01324B



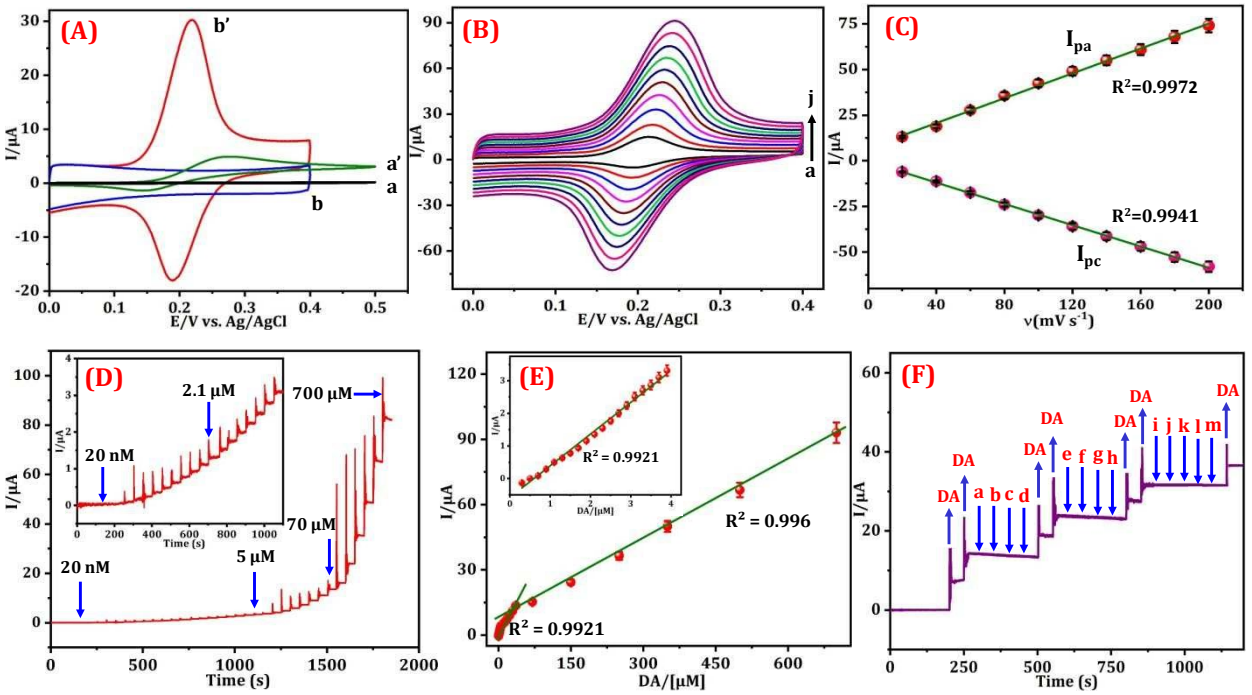


**Fig. 5.** (A) CV responses of bare GCE (a, a') and FMH/GCE (b, b') with the absence (a, b) and presence (a', b') of 200 μM DA in 0.05 M PBS (pH 7) at a scan rate of 50 mV $s^{-1}$. (B) CVs of FMH/GCE toward 200 μM DA in 0.05 M PBS (pH 7) with various sweep rates (20-200 mV $s^{-1}$; a→j) (n=3). (C) Calibration plot between the scan rate (ν) and the redox peak current ($I_{pa}$, $I_{pc}$) of DA. (D) Amperometric current responses of various concentration of DA in a stirred 0.05 M PBS (pH 7) on FMH modified electrode at 0.2 V. (E) The calibration plot for various DA concentrations and oxidation response current of DA (n=3). (F) I-t responses of FMH modified electrode toward 100 μM DA in the presence of various coexisting compounds UA (a), AA (b), CA (d), glu (e), cys (f), lys (g), Asp (h), $K^+$ (i), $Na^+$ (j), $Cl^-$ (k), $NO_3^-$ (l) and $SO_4^{2-}$ (m) in 0.05 M PBS (pH 7).

### *3.4. Electrocatalytic detection of CySH on FMH modified electrode*

#### *3.4.1. Electrocatalytic behaviour of FMH modified electrode towards CySH oxidation*

The electrochemical behaviour of FMH/GCE towards CySH in 0.05 M PBS (pH 7) was analyzed at a scanning range of 50 mV $s^{-1}$ by CV studies. Fig. 6A reveals the CVs of bare GCE and FMH/GCE in the presence and absence of 0.3 mM CySH, it was found that no obvious oxidation peaks were observed at bare GCE (curve a) and FMH/GCE (curve b) for without

View Article Online
DOI: 10.1039/D0TB01324B

addition of CySH. However, the CVs of bare GCE (a') in the presence of 0.3 mM CySH clearly indicates that the oxidation of CySH does not occurred at bare GCE due to poor catalytic behaviour. However, curve b' of Fig. 6A depicts that the well-defined anodic peak was noted at 0.16 and 0.46 V, respectively for FMH/GCE toward 0.3 mM CySH, indicating that the FMH could reduce the over potentials and increase the anodic peak current ($I_{pa}$; 27.34 μA) than the bare GCE. There is no reduction peak was noted during the reverse scan, indicates that the electro-oxidation of CySH is an irreversible, which proves that the LDH film had excellent adsorption capacity, thus could efficiently catalyze the oxidation of CySH. The enhanced current response should be ascribed to the nanostructure, high surface area and abundant active sites.

*3.4.2. Influence of scan rate towards CySH oxidation*

So as to know the kinetic reaction and the mechanism of the electrochemical oxidation of CySH on FMH/GCE, the effect scan rate was investigated via CV in 0.05 M PBS (pH 7). As depicted Fig. 6B demonstrates that the CV responses of 0.2 mM CySH gradually increases with increasing the scan rate from 20 to 200 mV $s^{-1}$. Furthermore, the anodic peak current ($I_{pa}$) values are linear relationship with the square root of the scan rate ($\nu^{1/2}$) and the corresponding correlation coefficient ($R^2$) is to be 0.9954, was revealed in Fig. 6C. These results imply that the electrochemical oxidation reaction of CySH is controlled by a diffusion process.[43] The anodic peak potentials of CySH shifts toward more positive direction with the increment of scan rates demonstrating the irreversible electrochemical oxidation and the rapid electron transfer kinetics at the electrode surface. Then the relationship between the anodic peak potentials ($E_{pa}$) of CySH and log of scan rate (log ν) is showed straight line, was revealed in Fig. S3D. As an irreversible oxidation process, the peak potential could be present by the following Eq. 5.[40]

$$E_p = A + 2.3RT/(1-\alpha)nF \log \nu \quad \text{---------- (5)}$$

Where, A is a constant, which related to with the formal electrode potential ($E_0$) and the standard rate constant at $E_0$. Then the electron transfers coefficient (α) value can be calculated from this Eq. 5, which describes the effect of electrochemical potential on the activation energy of an electrocatalytic reaction, and for most systems having the values

View Article Online
DOI: 10.1039/D0TB01324B

range from 0.3 to 0.7 s.[44] According to the slope of $E_{pa}$ vs. log ν, the calculated α value is to be 0.59. This result agrees with the direct electrochemical oxidation of CySH described in the following Eq. 6.[45]

$$2CySH \leftrightarrow CyS{-}SyC + 2e^- + 2H^+ \text{---------- (6)}$$

*3.4.3. Quantitative determination of CySH on FMH modified electrode*

To further ascertain the sensing performances for the quantitative detection of CySH on the FMH modified electrode, typical amperometric i-t technique was performed for the successive injection of CySH into stirred 0.05 M PBS (pH 7). Maximum current response for the oxidation of CySH was observed at 0.46 V and hence chosen as optimum potential for the quantitative amperometric experiments. Under ambient conditions, the quantitative analysis was performed at 50 s time intervals. As can be seen from the depicted Fig. 6C, the well-defined amperometric signals were observed with increase in the anodic current response with the increased concentration of CySH, which indicating that the more CySH reacted with the electrode surface. As seen, the developed electrode shows a rapid response to the injection of CySH, i.e. a steady state current is obtained after 2 s, which confirms the high electrocatalytic behaviour of the developed electrode. Moreover, a good two linear relationships were obtained with the $R^2$=0.9912 and $R^2$=0.9941, respectively, between the anodic peak current ($I_{pa}$) and the concentrations of CySH over a range of 30 nM-433 μM and 433 μM-6.67 mM (Fig.6D). The limit of detection (LOD) and limit of quantification (LOQ) toward CySH was calculated to be 9.6 nM and 32.03 nM, which suggests that the present study has great potential for diagnosis, due to the level of CySH in healthy plasma is about 240-360 μM.[46] Then the obtained analytical parameters were compared with previous reported CySH sensors based on the various nanomaterials (Table S2). These results confirming that the FMH modified electrode has been considered as a most promising electrocatalyst among the other 2D and 3D nanomaterial based electrochemical CySH biosensors. The developed assay platform not only have superior sensing ability on the aspect of broad linear-detection range, much better LOD and also it served as an alternative electrocatalyst over those of reported assays, due to the high cost of electrocatalyst and difficult synthetic procedures of previous reports.

View Article Online
DOI: 10.1039/D0TB01324B

*3.4.4. Interferents study towards CySH oxidation*

In order to alleviating, the more detailed information of FMH modified GCE toward CySH; the selectivity was evaluated by performing the amperometric i-t experiments. Exclusion of biological interferences is a major challenge, in order to the selectivity studies, the injection of 0.1 mM CySH and various possible interfering compounds such as aspartic acid (Asp), tryptophan (Trp), glycine (gly), glutathione (GSH), homocysteine (Hcy), ascorbic acid (AA), uric acid (UA), dopamine (DA), glucose (glu), $H_2O_2$, $Cl^-$, $SO_4^{2-}$, $Na^+$, $K^+$, $Fe^{2+}$ and $NH_4^+$, respectively, were injected in 0.05 M PBS (pH 7). The electroactive thiol containing compounds such Hcy, GSH are the main interferents for the detection of CySH in biological samples, because Hcy has similar chemical structure and also previous reports declares that it might be interfere in the sensing of CySH.[47] And also, the most important biological substances of AA and UA may often coexist with CySH in human fluids and physiological analysis. As shown Fig. 6E, the significant enhancement in the i-t responses were observed for the addition of 0.1 mM CySH. On the other hand, the negligible response current was noted with the successive injection of 1 mM (10 times higher concentration) possible interfering species of Asp (a), Trp (b), gly (c), Hcy (d), GSH (e), AA (f), UA (g), DA (h), $H_2O_2$ (i), glu (j), $Cl^-$ (k), $SO_4^{2-}$ (l), $Na^+$ (m), $K^+$ (n), $Fe^{2+}$ (o) and $NH_4^+$ (p), whereas, Hcy shows a faint amount of response current, hence do not interfere with the oxidation of CySH. These results confirm the excellent selectivity of the FMH modified electrode toward the tracking of CySH.

View Article Online
DOI: 10.1039/D0TB01324B



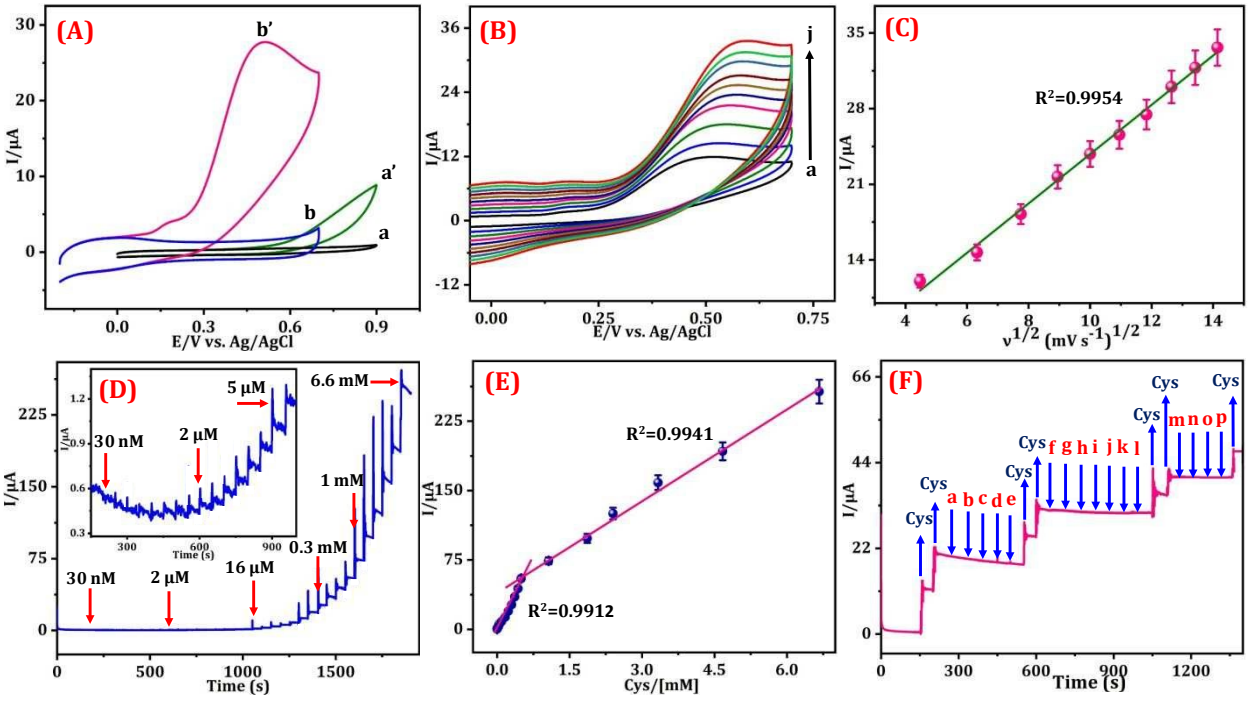


**Fig. 6.** (A) CV responses of bare GCE (a, a') and FMH/GCE (b, b') without (a, b) and with (a', b') 0.3 mM CySH in 0.05 M PBS (pH 7) at a scan rate of 50 mV $s^{-1}$. (B) CVs of different scan rates (20-200 mV $s^{-1}$; a→j) toward 0.3 mM CySH in 0.05 M PBS (pH 7) at FMH/GCE (n=3). (C) Calibration plot amongst the square root of scan rate ($\nu^{1/2}$) and oxidation peak current ($I_{pa}$) of CySH. (D) I-t responses of different concentration of CySH in a constantly stirred 0.05 M PBS (pH 7) on FMH modified electrode at an applied potential of 0.46 V. (E) The linear plot between different concentration of CySH and anodic current response (n=3). (F) I-t responses of 0.1 mM CySH in the presence of various interferences of Asp (a), Trp (b), gly (c), Hcy (d), GSH (e), AA (f), UA (g), DA (h), $H_2O_2$ (i), glu (j), $Cl^-$ (k), $SO_4^{2-}$ (l), $Na^+$ (m), $K^+$ (n), $Fe^{2+}$ (o) and $NH_4^+$ (p), on FMH modified electrode in 0.05 M PBS (pH 7) under constant stirring.

### *3.5. Real time tracking of CySH in human blood sample*

The point-of-care utility of the FMH based CySH sensor was further assessed by the tracking of blood CYSH. The samples were collected from three different healthy persons (named as Blood A, B, C) and it was examined by preparing 5 mL aliquots containing 15% of blood in 0.05 M PBS (pH 7). The prepared assay was transferred to an electrochemical cell and analyzed. As expected, the produced blood CySH levels of healthy persons were consistent with previous reports as well as theoretical concentrations (Table 1, Sample A-

View Article Online
DOI: 10.1039/D0TB01324B

C).[48] Moreover, the various concentration of CySH spiked blood samples were also analyzed with satisfactory results. To the conclude, the developed FeMn-LDHs based biosensor can be well suitable for the determination of blood CySH and also applicable for the practical analysis.

**Table 1.** Real time tracking of blood CySH at FMH modified electrode

| *Blood Sample* | *CySH Spiked (μM)* | *Found (μM)* | *RSD (%)* |
|---|---|---|---|
| *A* | 0 | 19.26 ± 0.023 | 1.26 |
| *B* | 0 | 18.23 ± 0.046 | 1.04 |
| *C* | 0 | 21.81 ± 0.031 | 1.32 |
| *D* | 5 | 24.3 ± 0.012 | 1.26 |
| *E* | 10 | 39.27 ± 0.01 | 1.41 |

*RSD- Relative Standard Deviation of three individual measurements*

### *3.6. Real time monitoring of DA in biofluids*

The developed sensor possesses a superior linear range (50 nM to 3.9 μM and 3.9 μM to 700 μM), which is highly applicable for the fluctuation of DA concentrations from low to high in biological range (such as human cerebrospinal fluid (between 0.5 and 25 nM); brain (between 0.01 and 1 μM)). The excessive level of DA can cause severe diseases, and cell damages, about 20-50 μM of DA can halt neuronal NMB cell growth. A concentration of DA exceeds over 100-300 μM can be a neurotoxic and cause apoptosis.[49] On account of this, and the ability of the developed FMH toward DA sensor, we have design to demonstrate the application of this assay, the level of DA in dopamine injection solution, human serum and urine samples were monitored, via amperometric measurements by using standard addition technique. The dopamine injection solution was collected from the Taipei hospital and the serum and urine samples were collected from the healthy volunteers. Prior to start the experiments, the amount of known DA concentrations were successfully spiked into these samples. The amperometric i-t technique was studied and the obtained results were listed in Table. 2 then the calculated recoveries of these samples were 99.6–102.8 (dopamine injection solution), 99–99.4 % (Blood serum), and 99.3–99.6 % (urine) respectively, toward

View Article Online
DOI: 10.1039/D0TB01324B

DA detection. From this result, the developed FMH modified electrode had excellent practicability.

**Table 2. Results of determination of DA in biological fluids.**

| *Sample* | *Spiked (μM)* | *Found (μM)* | *Recovery (%)* | *RSD (%) (n=3)* |
|---|---|---|---|---|
| *Dopamine injection solution* | 10 | 9.96 | 99.6 | 0.15 |
| | 20 | 20.56 | 102.8 | 0.07 |
| | 30 | 29.92 | 99.73 | 0.14 |
| *Blood serum* | 10 | 9.94 | 99.4 | 0.1 |
| | 20 | 19.88 | 99.4 | 0.08 |
| | 30 | 29.7 | 99 | 0.13 |
| *Urine* | 10 | 9.93 | 99.3 | 0.05 |
| | 20 | 19.87 | 99.35 | 0.13 |
| | 30 | 29.9 | 99.6 | 0.12 |

## 4. Conclusion

In summary, we have developed a time controlled hydrothermal synthesis of nanostructured FeMn LDHs (FMH) with various physiochemical attributes (hexagonal plate, cube, sphere). The FMH nanocubes offered the lowest particle size, highest surface area, and highest pore diameter among the three-nanostructured materials. These intrinsic advantages could be enhancing their electrocatalytic activity with the high heterogeneous rate constant ($7.81\times10^{-6}$ cm $s^{-1}$), high electroactive surface area (0.3613 $cm^2$), and low impedance (96 Ω). The FMH nanocubes based electrochemical dopamine (DA) and Cysteine (CySH) detection achieved good linearity (20 nM-700 μM and 30 nM-9.6 mM) with low detection limit (5.3 nM and 9.6 nM). Based on these advantages, it was applied to the real world sensing of blood CySH levels and DA levels in various biological fluids with admirable consistency. Hence, the developed assay platform could potentially be used as an excellent electrode modifier for the real-time determination of diagnostic test strips for measuring the level of CySH in blood and DA in bio fluids.

View Article Online
DOI: 10.1039/D0TB01324B

## ACKNOWLEDGEMENT

The authors gratefully acknowledge the financial support of the Ministry of Science and Technology, Taiwan through contract no. MOST 107-2113-M-027-005-MY3.

## ASSOCIATED CONTENT

### Supplementary Information

Additional information (Materials and methods, electrode fabrication, BET analysis for as prepared material, electrochemical studies for the sensing performances of developed electrode, comparison table for both DA and CySH sensor and the table for real time determination of DA and CySH) is given in supplementary information.

### Conflicts of interest

There are no conflicts to declare.

View Article Online
DOI: 10.1039/D0TB01324B



## Reference

1. H. Jin, C. Zhao, R. Gui, X. Gao and Z. Wang, *Analytica chimica acta*, 2018, **1025**, 154-162.
2. H. Song, H. Zhao, X. Zhang, Y. Xu, X. Cheng, S. Gao and L. Huo, *Biosensors and Bioelectronics*, 2019, **133**, 250-257.
3. Y.-S. He, C.-G. Pan, H.-X. Cao, M.-Z. Yue, L. Wang and G.-X. Liang, *Sensors and Actuators B: Chemical*, 2018, **265**, 371-377.
4. I. Suzuki, M. Fukuda, K. Shirakawa, H. Jiko and M. Gotoh, *Biosensors and Bioelectronics*, 2013, **49**, 270-275.
5. Q. Qian, J. Deng, D. Wang, L. Yang, P. Yu and L. J. A. c. Mao, *Analytical chemistry*, 2012, **84**, 9579-9584.
6. S. Ge, M. Yan, J. Lu, M. Zhang, F. Yu, J. Yu, X. Song and S. J. B. Yu, *Biosensors and Bioelectronics*, 2012, **31**, 49-54.
7. Y. Zhang, J. Jiang, M. Li, P. Gao, Y. Zhou, G. Zhang, S. Shuang and C. J. T. Dong, *Talanta*, 2016, **161**, 520-527.
8. A. N. Patel, S.-y. Tan, T. S. Miller, J. V. Macpherson and P. R. Unwin, *Analytical chemistry*, 2013, **85**, 11755-11764.
9. N. Yang, H. Song, X. Wan, X. Fan, Y. Su and Y. J. A. Lv, *Analyst*, 2015, **140**, 2656-2663.
10. J.-L. Chen, X.-P. Yan, K. Meng and S.-F. Wang, *Analytical chemistry*, 2011, **83**, 8787-8793.
11. B. K. Rani, and S. A. J. B. John, *Biosensors and Bioelectronics*, 2016, **83**, 237-242.
12. C. Muzzi, E. Bertocci, L. Terzuoli, B. Porcelli, I. Ciari, R. Pagani and R. Guerranti, *Biomedicine & pharmacotherapy*, 2008, **62**, 253-258.
13. G. Chwatko, E. Kuźniak, P. Kubalczyk, K. Borowczyk, M. Wyszczelska-Rokiel and R. J. A. M. Głowacki, *Analytical Methods*, 2014, **6**, 8039-8044.
14. J. A. Ribeiro, P. M. Fernandes, C. M. Pereira and F. Silva, *Talanta*, 2016, **160**, 653-679.
15. M. Alam, A. M. Asiri, M. M. Rahman and M. Islam, *Materials Chemistry and Physics*, 2020, **244**, 122740.

View Article Online
DOI: 10.1039/D0TB01324B



16. W. J. Barreto, S. R. Barreto, R. A. Ando, P. S. Santos, E. DiMauro and T. Jorge, *Spectrochimica Acta Part A: Molecular and Biomolecular Spectroscopy*, 2008, **71**, 1419-1424.
17. A. Aziz, M. Asif, M. Azeem, G. Ashraf, Z. Wang, F. Xiao and H. Liu, *Analytica chimica acta*, 2019, **1047**, 197-207.
18. C.-H. Chen and S.-C. Luo, *ACS applied materials & interfaces*, 2015, **7**, 21931-21938.
19. Y. Huang, Y.-E. Miao, S. Ji, W. W. Tjiu and T. Liu, *ACS applied materials & interfaces*, 2014, **6**, 12449-12456.
20. S.-Y. Yu, Y. Gao, F.-Z. Chen, G.-C. Fan, D.-M. Han, C. Wang and W.-W. J. S. Zhao, *Sensors and Actuators B: Chemical*, 2019, **290**, 312-317.
21. M. M. Rahman, S. B. Khan, G. Gruner, M. S. Al-Ghamdi, M. A. Daous and A. M. J. E. A. Asiri, *Electrochimica Acta*, 2013, **103**, 143-150.
22. N. I. Chandrasekaran and M. Manickam, *Sensors and Actuators B: Chemical*, 2019, **288**, 188-194.
23. F. Yan, D. Guo, J. Kang, L. Liu, C. Zhu, P. Gao, X. Zhang and Y. Chen, *Electrochimica Acta*, 2018, **283**, 755-763.
24. A.-L. Wang, H. Xu and G.-R. Li, *ACS Energy Letters*, 2016, **1**, 445-453.
25. Z. P. Xu, J. Zhang, M. O. Adebajo, H. Zhang and C. Zhou, *Applied Clay Science*, 2011, **53**, 139-150.
26. J. Zhou, M. Min, Y. Liu, J. Tang and W. Tang, *Sensors and Actuators B: Chemical*, 2018, **260**, 408-417.
27. J. Chen, Q. Sheng, Y. Wang and J. J. E. Zheng, *Electroanalysis*, 2016, **28**, 979-984.
28. Y. Wang, W. Peng, L. Liu, F. Gao and M. J. E. a. Li, *Electrochimica acta*, 2012, **70**, 193-198.
29. Y. Zhang, J. Tian, S. Liu, L. Wang, X. Qin, W. Lu, G. Chang, Y. Luo, A. M. Asiri and A. O. Al-Youbi, *Analyst*, 2012, **137**, 1325-1328.
30. F. Song and X. J. N. c. Hu, *Nature communications*, 2014, **5**, 4477.
31. T. Hibino and H. J. A. C. S. Ohya, *Applied Clay Science*, 2009, **45**, 123-132.
32. Y. Ruan, X. Jia, C. Wang, W. Zhen and X. Jiang, *Chemical communications*, 2018, **54**, 11729-11732.

View Article Online
DOI: 10.1039/D0TB01324B



33. G. Huang, K.-L. Zhang, S. Chen, S.-H. Li, L.-L. Wang, L.-P. Wang, R. Liu, J. Gao and H.-H. Yang, *Journal of Materials Chemistry B*, 2017, **5**, 3629-3633.
34. G. I. Waterhouse and M. R. Waterland, *Polyhedron*, 2007, **26**, 356-368.
35. H. M. Marwani, M. M. Rahman, S. B. Khan, A. M. Asiri, K. A. Alamry, M. A. Rub and M. T. S. J. M. R. B. Chani, *Materials Research Bulletin*, 2014, **51**, 287-294.
36. M. Annalakshmi, P. Balasubramanian, S.-M. Chen and T.-W. Chen, *Microchimica Acta*, 2019, **186**, 265.
37. R. Sukanya, M. Sakthivel, S.-M. Chen and T.-W. Chen, *Sensors and Actuators B: Chemical*, 2018, **269**, 354-367.
38. P. Balasubramanian, M. Annalakshmi, S.-M. Chen and T.-W. Chen, *Ultrasonics sonochemistry*, 2019, **50**, 96-104.
39. W.-C. Liu, H.-K. Lin, Y.-L. Chen, C.-Y. Lee and H.-T. Chiu, *Acs Nano*, 2010, **4**, 4149-4157.
40. A. J. Bard, L. R. Faulkner, J. Leddy and C. G. Zoski, *Electrochemical Methods*, 1980, **482**, 580-632.
41. L.-H. Liu, C.-Q. Duan and Z.-N. Gao, *Croatica Chemica Acta*, 2010, **83**, 409-414.
42. A. Muthaiah, P. Balasubramanian, S. M. Chen, T.-W. Chen and P.-H. Lin, *Inorganic Chemistry Frontiers*, 2019.
43. C. Deng, J. Chen, X. Chen, M. Wang, Z. Nie and S. J. E. A. Yao, *Electrochimica acta*, 2009, **54**, 3298-3302.
44. Y.-T. Lai, A. Ganguly, L.-C. Chen and K.-H. J. B. Chen, *Biosensors and Bioelectronics*, 2010, **26**, 1688-1691.
45. M. Zhou, J. Ding, L.-p. Guo and Q.-k. J. A. C. Shang, *Analytical Chemistry*, 2007, **79**, 5328-5335.
46. H. Refsum, P. Ueland, O. Nygård and S. J. A. r. o. m. Vollset, *Annual review of medicine*, 1998, **49**, 31-62.
47. F. Chen, J. Zhang, W. Qu, X. Zhong, H. Liu, J. Ren, H. He, X. Zhang and S. J. S. Wang, *Sensors and Actuators B: Chemical*, 2018, **266**, 528-533.
48. H. Agarwalla, N. Taye, S. Ghorai, S. Chattopadhyay and A. J. C. C. Das, *Chemical Communications*, 2014, **50**, 9899-9902.
49. Y.-M. Zhang, P.-L. Xu, Q. Zeng, Y.-M. Liu, X. Liao and M.-F. Hou, *Materials Science and Engineering: C*, 2017, **74**, 62-69.